HIGHLY CONFIGURABLE GNSS/STR/INS INTEGRATION FOR SPACE TRANSPORTATION SYSTEMS

Gonzalo Zamora-Caballero	AOCS/GNC Engineer, SENER, Seville, Spain. gonzalo.zamora@aeroespacial.sener
Sergio Ramírez Navidad	Head of the Hybrid Navigation Units Business Line, SENER, Madrid, Spain. sergio.ramirez@aeroespacial.sener
Juan Cañizares Gómez de Terreros	AOCS/GNC Engineer, SENER, Seville, Spain. juan.canizares@aeroespacial.sener
Silvia Diaz Ribera	Project Manager, SENER, Madrid, Spain, silvia.diaz@aeroespacial.sener
Mariano Sánchez Nogales	Business Development Manager, SENER, Madrid, Spain, mariano.sanchez@aeroespacial.sener
Gianluca Curti	System/GNC Engineer, ESA ESRIN, Via Galileo Galilei, 1, 00044 Frascati RM, Italy, gianluca.curti@esa.int

ABSTRACT

Typical hybrid navigation units combine high-frequency but drifting measurements, such as those provided by an Inertial Measurement Unit (IMU), with low-frequency but bounded measurements, such as the ones provided by a GNSS receiver. In the context of space navigation systems, including the new navigation unit of the VEGA-C, NAVIGA, a loosely coupled GNSS/IMU architecture is traditionally employed to combine and hybridize these signals, mainly driven by simplicity and processing constraints. In contrast, the NAVIGA Evolution (NAVIGA-EVO) navigation system upgrades the NAVIGA loosely coupled architecture to a tightly coupled hybrid solution. Furthermore, this unit integrates a multi-sensor fusion system, hybridizing attitude measurements from a star tracker (STR).

This paper presents the architecture, design and performance of the NAVIGA-EVO system, which includes new features and enhances the performances of the baseline NAVIGA unit. Envisaged for the GNC subsystem of VEGA-C and Space Rider (SR), the system is tailored to address new use cases and scenarios beyond LEO, including Geostationary Transfer Orbit (GTO) and Earth re-entry. To achieve this, the unit is capable of operating in high altitude orbits and incorporates capabilities provided by the GNSS sensor, including dual-frequency and dual-RF antenna support.

In this work, advanced processing algorithms have been developed and implemented to enable tight hybridization and STR integration, building upon a loosely coupled configuration and ensuring compatibility across all configurations. The unit processes and hybridizes the GNSS raw data together with the IMU data. The tight hybridization architecture also receives, processes and hybridizes external attitude data from a STR. The architecture is designed to maximize the exploitation of measurement data by effectively combining information from multiple sensors. To ensure robustness, the data fusion operates with a fault detection, isolation and recovery algorithms.

Finally, this paper presents a comparative analysis of the performance of the loose and tight hybridization schemes, with and without the inclusion of STR data. Navigation performance results are

Doi: 10.82124/CEAS-GNC-2026-015 **CEAS-GNC-2026-015**

evaluated for high-altitude (GEO) VEGA-C missions and Space Rider trajectories, including the re-entry phase. The results conclude that the tightly coupled hybridization not only enhances system robustness system but also delivers better performance outcomes.

Keywords: NAVIGA, GNSS, tight, star tracker, dual-antenna, dual-frequency.

Nomenclature

x_0^+	=	initial state
x_{k-1}^+	=	final updated state of previous time step
x_k^-	=	propagated state of current time step
F_{k-1}	=	state transition matrix between time steps
P_{k-1}^+	=	updated covariance matrix at previous time step
P_k^-	=	propagated covariance matrix at current time step
Δx_k^-	=	propagated error state at current time step
Δx_k^+	=	updated error state at current time step
P_k^+	=	updated covariance matrix at current time step
Σ_k	=	Square-root matrix of covariance matrix at current time step
x_k^+	=	updated state at current time step
F_k	=	State Transition Matrix at current time step
h	=	Altitude of the space vehicle
E	=	Relative elevation angle of the GNSS satellite
d_I	=	Ionospheric delay

1 Introduction

The VNE (VEGA Navigation Equipment) is an electronic sensing/processing unit providing a navigation solution to be integrated into the GNC subsystem of the VEGA-C launcher and Space Rider (the associated extended mission, hereafter recalled as SR). The unit is devoted to providing a complete set of reliable navigation data consistent with the GNC subsystem needs for the different phases: launcher, orbital and re-entry phases of the associated missions.

For the VEGA-C mission the unit will be physically integrated into the equipment bay of the VEGA launcher on 4^{Th} stage. For Space Rider, each of the vehicles composing the system will have physically attached at least one VNE unit. In particular, the Space Rider system is composed of the AVUM Orbital Module (AOM) and the Re-entry Module (RM) [1].

The Equipment shall generate suitable data such as attitude, velocity and position according to the selected inertial reference frame. This information will be provided to the main On-Board Computer (O+BC) for integration together with the rest of the sensor data for navigation computing.

The unit consists of an equipment capable of processing and integrating the information coming from two subsystems: an Inertial Measurement Unit (IMU) and Global Navigation Satellite System (GNSS). The functional outcome of this data processing is a robust hybrid navigation solution that fuses the stand-alone solutions.

Looking for an extension of VNE capabilities, the NAVIGA Evolution (NAVIGA-EVO) project was created, in order to enable high-altitude and re-entry operations. To achieve that purpose, following technological building blocks are required: Tight GNSS Hybridization, GNSS Dual-Antenna Processing, GNSS Dual-Frequency Processing, and Star Tracker Hybridization.

These technical objectives have an additional one, which is related to the compatibility to the VNE baseline configuration. This is required to facilitate, in the future, the possible parallel production of NAVIGA and NAVIGA-EVO units.

The objective of this paper is to present the innovative data fusion algorithms implemented in the NAVIGA-EVO unit. As remarked, the baseline of the project is based on the NAVIGA unit framework [2], subsequently incorporating the different evolutions and enhancements of the project to support complex mission profiles.

Tightly coupled GNSS solutions enhance navigation robustness by eliminating architectural dependency on the classical position and velocity hybridization [3]. The fundamental principles for raw data hybridization are detailed in [4]. Previous research [3]**¡Error! No se encuentra el origen de la referencia.** demonstrated the efficacy of tightly coupled integration for vehicles in high-dynamic environments. Specifically, [3] applied an Extended Kalman Filter (EKF) to space transportation systems included integrated measurements (Time-Difference Carrier Phase, TDCP), while [6] and [7] explored the hybridization of pseudorange and pseudorange-rate measurements. Several authors as [8], [9], [10] deal with the usage of TDCP measurements in real-time applications as missiles.

Some of the additional capabilities of the unit are deeply analyzed in the literature. The integration of Star Tracker (STR) data is a cornerstone of the NAVIGA-EVO unit. The Multiplicative Extended Kalman Filter (MEKF) remains the standard approach for STR-based attitude estimation [11][12]. The primary novelty of this research lies in a multi-hybridization architecture that optimizes state estimation while managing high-fidelity sensor simulations, including inherent delays and latencies. To address the challenge of delayed measurements in complex environments, this paper draws on methodologies proposed by Larsen [13] and Alexander [14], optimizing the introduction of combined delayed data due to sensor processing requirements. Furthermore, the NAVIGA-EVO architecture employs a unified, multi-rate architecture that maintains compatibility with legacy systems. In the literature, [15] analyzes several existing approaches to incorporate delayed measurements. In [14], the authors set the basis for a system where state propagation occurs at a higher frequency than sensor updates to ensure GNC stability. In this text, the data fusion algorithms are divided into three different frequencies according to the task's priority and sensor frequencies.

The manuscript is organized as follows: Section 3 establishes the operational context by describing the mission cases that necessitate these enhanced functionalities. Within this framework, Section 3.2 details the navigation architecture, focusing specifically on loose (3.3) and tight (3.4) hybridization strategies and the multi-sensor data fusion scheme (3.5). Section 4 introduces the Fault Detection, Isolation and Recovery (FDIR) architecture and Section 5 details the Software-in-the-Loop (SIL) implementation, describing the simulation environment and the integration of the flight software. Section 6 presents a comprehensive analysis of the simulation results, where diverse unit configurations are leveraged to evaluate and compare performance across a range of mission scenarios. Finally, Section 7 provides concluding remarks and discusses the roadmap for future work.

2 Mission Use Cases

As mentioned in the previous section, the NAVIGA Evolution project aims to enhance the VNE unit, and to extend its capabilities to serve the following use cases:

2.1 High Altitude Injection

The reference trajectory for the high-altitude use case is a VEGA modified trajectory not considering any payload release, provided by ESA. This trajectory is a GTO-GEO one that includes all the launcher phases, from missile phase to orbit injection. The objective of the trajectory is to validate the following technical objectives: GNSS dual-antenna processing, tight GNSS hybridization and STR hybridization and high-altitude configuration/operation.

2.2 Re-Entry Trajectory

The reference trajectory for the re-entry use case is a SR-RM, coming from the VNE project. This trajectory is an equatorial one that includes all the re-entry phases of the SR-RM vehicle, from orbit coasting till landing. The objective of the trajectory is to validate the Tight GNSS Hybridization and the GNSS Dual-Frequency Processing technical objective.

3 Navigation Architecture

In this section the full navigation architecture is described. Subsection 3.1 presents the different modes describing the different phases faced by the two trajectories of interest, as well as the possible initial alignments. In Subsection 3.2, the core data fusion architecture is decomposed in the different functions which make it compatible with NAVIGA and extend its capabilities to the EVO performances.

3.1 Navigation Modes

The VNE unit includes several modes as well as configurations such as missile, orbital, re-entry, coasting and high altitude. The transition between different alignment modes is determined based on the three possible alignments or initializations:

- Nominal alignment: this transition is initiated from the off mode coarse alignment, using the coarse alignment, followed by the fine alignment, before finally implementing the flight telecommand and executing the flight mode.
- Fast alignment: this transition begins from the off with the fine alignment and subsequently proceeds to implement the flight telecommand and execute the flight mode.
- Dynamic alignment: in this case, the transition is directly initialized from the off mode to the flight mode.

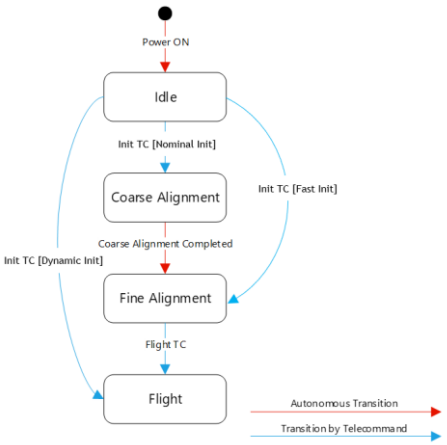

Fig. 1: General schematic of the Navigation Modes.

3.2 Data Fusion Functions

The functions implemented in the Data Fusion (DF) compose a triple rate Kalman Filter [16]. If a single rate data fusion is used, the execution time of the hybrid navigation will be constant during the inertial propagation, but it will present important peaks in the cycles when the GNSS measurement is fused. Hence, there will be a significant amount of computational resources unused when there are no GNSS measurements available.

The triple rate Kalman Filter scheme is based on the idea that data fusion tasks are run in different processes at different frequencies, low rate, medium rate and high rate. The EKF is performed now at low-rate process. On the other hand, the inertial propagation is carried out at high rate whereas it is the covariance propagation function which is performed at medium rate, as well as the additional calculus necessary for the integration of the delayed KF updates. This architecture increases the number of operations during the inertial and covariance propagation but reduces significantly the execution time peaks corresponding to the EKF updates.

The data fusion functions are described as:

1) Coarse Alignment Function (CAF): in charge of calculating the initial attitude using the IMU measurements, by means of levelling and gyro-compassing processes.
2) Fine Alignment Filter (FAF): implements a Kalman Filter (KF) in order to align and calibrate the IMU measurements using virtual on-ground measurements.
3) Inertial Propagation Function (IPF): in charge of updating the navigation information with the most recent data provided by the Inertial Navigation System (INS). The rate of execution of this task will be directly related to the rate used by the On-Board Computer (OBC) to request the navigation data.
4) Data Fusion Post-Processing (DPP): its objective is to have a modular architecture that has an independent function to obtain the navigation data required by the vehicle OBC.
5) Covariance Propagation Function (CPF): in charge of propagating the covariance matrix. It is run at a lower frequency in order to optimize the memory and CPU usage.
6) GNSS Hybridization Filter (GHF): implements a KF that computes the innovation each time there is a new set of GNSS observables (position, velocity and time solution).
7) GNSS Tight Hybridization Filter (THF): implements a KF that computes the innovation each time there is a new set of GNSS raw observables.
8) Star Tracker Hybridization Filter (SHF): implements a KF that computes the innovation each time there is a star tracker measurement.

3.2.1 Navigation Logic

The main functions of the DF are general, however, depending on the mode, some functions are active or not. The general formulation follows the following scheme which is depicted in Fig. 2.

The data fusion architecture process is detailed in the following steps. After the initialization of the state (x_0^+), the main navigation loop applies:

- IPF: Propagate estimated state from previous time $(k-1)$ to current time (k):

$$\mathrm{x}_{\mathrm{k}-1}^{+} \rightarrow \mathrm{x}_{\mathrm{k}}^{-} \tag{1}$$

- CPF: Use $\mathrm{x}_{\mathrm{k}-1}^{+}$ to compute discrete state transition matrix $\mathrm{F}_{\mathrm{k}-1}$.
- CPF: Propagate state error covariance from previous time $(k-1)$ to current time (k):

$$P_{k-1}^{+} \rightarrow P_{k}^{-} \tag{2}$$

- Sequential Schmidt-Kalman Filter innovation to compute updated delta-state at current time:

$$\Delta x_{k}^{-} \rightarrow \Delta x_{k}^{+} \tag{3}$$

This step is common but differs depending on the five possible EKF hybridization functions: FAF, GHF, GHF+SHF, THF and THF+SHF. In all cases a sequential EKF is employed to reduce software computational cost of the classical Kalman gain [4][17].

- Correct delta-state delay due to EKF execution delay and update covariance:

$$P_{k}^{-} \rightarrow P_{k}^{+} \tag{4}$$

- Update state using delta-state:

$$x_{k}^{-} \oplus \Delta x_{k}^{+} = x_{k}^{+} \tag{5}$$

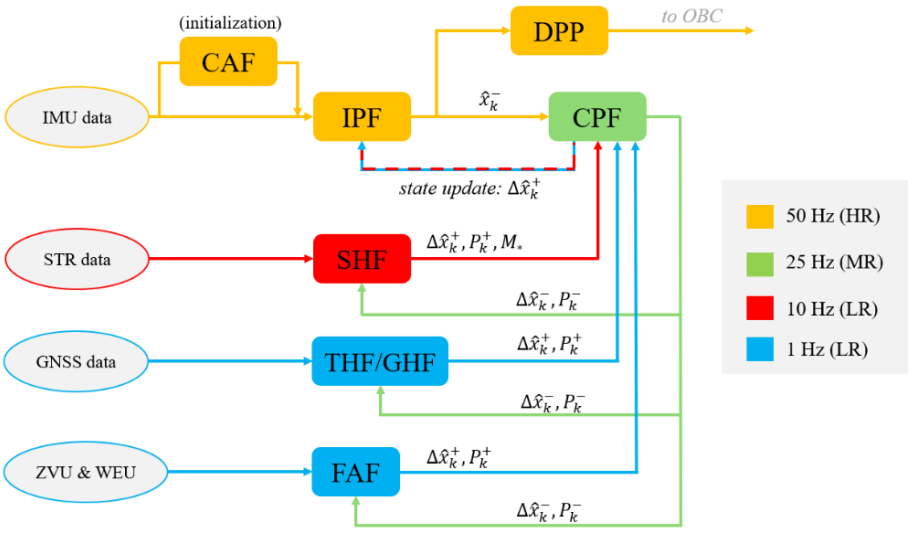

Fig. 2: Architecture of DF functions.

The full state propagated by the hybrid INS/GNSS/STR filter includes:

1. Navigation states: the position, velocity and attitude of the vehicle.
2. Receiver clock states: bias and clock of the GNSS receiver clock.
3. IMU parameter states: the accelerometer and gyro calibration parameters.
4. GNSS states: channel biases of pseudorange, pseudorange-rate, time-differenced carrier phase measurements, atmospheric correction scale factors, time-difference bias between GPS and GALILEO satellites, delayed GNSS receiver antenna position (ECI frame).
5. STR measurement bias in order to improve the attitude and gyroscope parameters estimation.

The IMU calibration parameters are related to the IMU error model, while the clock parameters are related to the onboard clock state model. The full state is summarized in Table 1.

In Table 1, a distinction is made between estimated and considered variables. This distinction arises from the fact that, in the Schmidt–Kalman filter approach [18], certain state elements are not directly estimated but are treated as considered variables in terms of their covariance. This means that these states values are not affected by the injection of new observations: their value is simply propagated, and their covariance increases according to their process noise, reflecting the presence of error residuals whose

estimation does not improve the performance of the filter. The notation *estimated/considered* refers to cases in which a variable may be either estimated or considered, depending on the sensor filter employed, namely the THF or SHF. Note that whenever a state is observed or well estimated using some measurement update, it needs to be at least considered in the rest of filters for covariance consistency.

Table 1: Full system state summary.

Symbol	Description	Size	Index	Filter
r_I	Position in ECI frame	[3]	1:3	Estimated
v_I	Velocity in ECI frame	[3]	4:6	Estimated
$q_{I\to B}$	Quaternion from ECI to Body frame	[4]	7:10	Estimated
b_r	GNSS receiver clock bias	[1]	11	Estimated
d_r	GNSS receiver clock drift	[1]	12	Estimated
b_A	Accelerometer bias in Body frame	[3]	13:15	Estimated/Considered
b_G	Gyro bias in Body frame	[3]	16:18	Estimated/Considered
s_A	Accelerometer scale factor error	[3]	19:21	Considered
s_G	Gyro scale factor error	[3]	22:24	Considered
m_A	Accelerometer misalignment errors	[6]	25:30	Considered
m_G	Gyro misalignment errors	[6]	31:36	Considered
α_G	Gyro non-gravitational sensitivity error	[3]	37:39	Ignored
b_ρ	Channel PR measurement bias	[16]	40:55	Estimated
$b_{\dot\rho}$	Channel PRR measurement bias	[16]	56:71	Considered
$b_{\Delta\rho}$	Channel TDCP measurement bias	[16]	72:87	Considered
s_T	Tropospheric uncertainty scale-factor	[1]	88	Considered
s_I	Ionospheric uncertainty scale-factor	[1]	89	Considered
r_{ant_d}	Delayed state of GNSS antenna position	[3]	90:92	Considered
b_{STR}	STR measurement bias in STR frame	[3]	93:95	Considered

3.3 Loose Hybridization

The loose hybridization function implements the classical formulation of the IMU/GNSS hybrid algorithm: GNSS position and velocity in ECEF from the GNSS Position, Velocity, and Time (PVT) solution are fused with the inertial integration. In this formulation it is assumed that the position and velocity of the receiver are computed at reception time. Nonetheless, the latency delay of the GNSS is corrected by extrapolating the measurements to the current navigation epoch [13].

3.4 Tight Hybridization

Rather than utilizing the pre-computed PVT solution to correct the inertial propagation, the tightly coupled hybridization directly makes use of the so called GNSS raw measurements: pseudorange (PR), pseudorange-rate (PRR) and carrier phase (CP). These observables are directly acquired from the GNSS unit. Avoiding GNSS receiver's internal navigation solver, the navigation is more robust, eliminating the dependency on the PVT problem requirement for a minimum of four satellites to maintain a navigation fix . However, this method also increases the dimensionality of the measurement model and the overall system complexity.

In this formulation of the IMU/GNSS tightly coupled hybrid algorithm, three types of measurements are employed: PR, PRR and time-differenced carrier phase (TDCP). These three allow 2 types of possible combinations of measurements: PRR+RR and PRR+TDCP, with the latter offering the highest accuracy.

3.4.1 TDCP Hybridization

The TDCP measurement is obtained from the accumulation of the phase increments from the carrier tracking loop [3]. According to [4], carrier-phase positioning can give centimeter accuracy for real-time navigation and millimeter accuracy for surveying and geodesy applications. Time-differentiation of the carrier phase cancels the influence of the ambiguity term associated with this magnitude.

However, treating TDCP as an integrated measurement implies the usage of a model that differentiates the carrier-phase-based pseudorange (carrier phase multiplied by the carrier wavelength) between the start and end of a discrete integration interval. In high-dynamics scenarios, the common assumption of a constant velocity (or "average" state) over the interval is insufficient due to significant vehicle maneuvers. To maintain filter consistency, the hybridization architecture must accurately account for the delayed antenna position. This is achieved through two distinct methodological approaches evaluated in this study. The first approach involves storing the STM between measurement epochs. The STM is then utilized to back-propagate the current estimate and compute the delayed state corresponding to the previous measurement [8]. Alternatively, the second approach introduces an additional state vector, representing the delayed GNSS antenna position. This state is reset following each Kalman update, based on [3].

3.4.2 Latency correction

GNSS observation measurements are characterized by a low update rate and significant latency. In such systems, measurements are not available to the filter instantaneously. They arrive with a delay of D cycles with respect to the navigation frequency. In order to incorporate GNSS measurements into the filter described, a correction must be applied to the propagated state.

Extrapolating the GNSS position and velocity as described in [13] and Section 3.3 cannot be applied due to the lack of continuous access to satellite ephemeris data at every integration sub-step. According to [16], delaying the entire error-state filter (both state and covariance) to the acquisition time requires the least computational effort. The filter update is obtained at the Pulse-Per-Second (PPS) acquisition timestamp. The updated error-state and covariance matrix are then forward-propagated to the current real-time navigation epoch using the accumulated State Transition Matrix (STM).

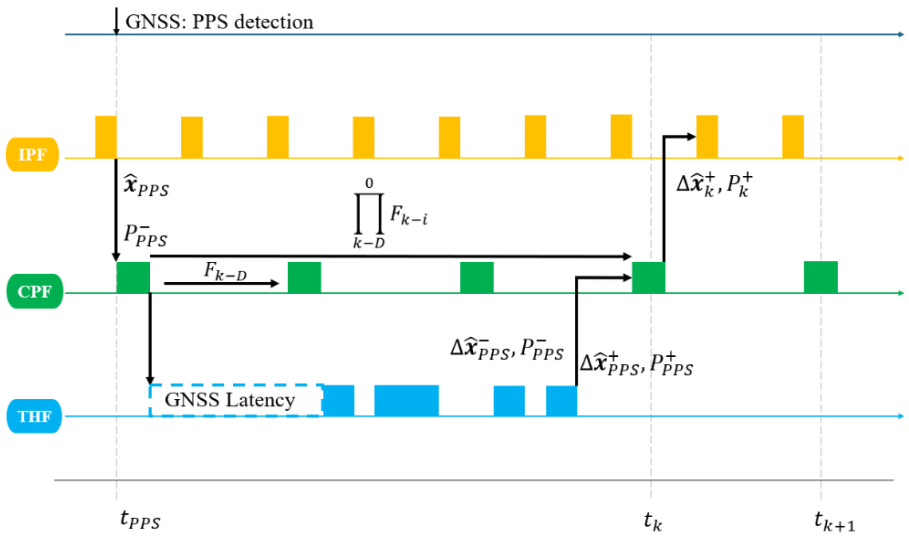

Fig. 3: Triple rate Kalman Filter with tighly information delayed.

3.4.3 Correction of errors

The mission profiles associated with the EVO performances lead to the elaboration of more complex tight models. Navigating trajectories beyond Low Earth Orbit (LEO) requires correcting for signal disruptions and atmospheric delays. The GNSS tight hybridization has been improved to correct different delays which can interfere and disrupt the GNSS signals and GNSS solutions.

The tightly coupled measurements are computed as geometric or true measurements; however, several errors can affect or modify these variables. Measuring errors may originate from a variety of sources.

In this work, several effects are considered such as: Sagnac effect [4]; ephemeris errors; relativistic effects (cross-linking); clock errors biases (in receiver and satellites); atmospheric delays: troposphere and ionosphere [20]; and other atmospheric errors such as ionospheric bending [21]; and satellite clock offsets (Timing Group Delay and Broadcast Group Delay). The main objective is to enhance the unit's capability to hybridize the maximum number of raw measurements under any operational condition. This represents a significant advantage over the conventional loose architecture, which requires tracking of at least four satellites. To account for these errors, the state vector is augmented to include measurement biases and scale factors, thereby considering the tropospheric and ionospheric residuals within the navigation state.

In this work, the ionospheric model is extended from the classical Montenbruck correction model [20], limited to low altitudes (LEO satellites) and positive elevation cases. Particularly, it is extended throughout geometrical simplifications to account for trajectories which arrive at GEO. In these cases, the relative position of the satellites with respect to the space vehicle makes their relative elevation (E) to be negative and the signal traverses completely the ionosphere. In this situation, the geometry of the problem allows the delay to be approximated by calculating the projection of the GNSS antenna vector to the line joining the space vehicle and the observed satellite. Due to symmetry, the total delay (d_I) can be estimated as twice the delay (Fig. 4) that would occur if the space vehicle were positioned at this projected point (d_I^*), assuming symmetrical deviation for signal paths that completely traverse the Ionosphere.

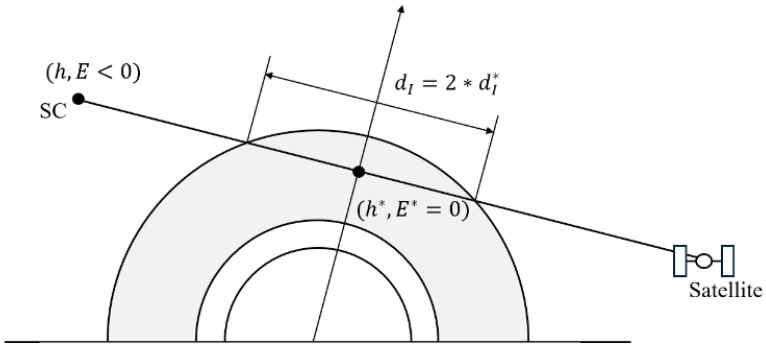

Fig. 4: Extended ionospheric model.

In this case, a secondary ionospheric effect arises due to the change of refractive index through the different layers of the ionosphere, inducing the ray-path bending of the electromagnetic wave [21]. This phenomenon can introduce pseudorange errors of several tens of meters. Due to its highly non-linear nature, this error is difficult to correct using simplified models within the EKF. Nonetheless, incorporating these affected measurements into the tight hybridization architecture is critical for high-altitude navigation. At these altitudes, the number of available GNSS observations is severely limited. Including satellites whose signals must traverse the ionosphere, even if they carry higher residual errors, maintain the hybridized navigation in regions where the filter would otherwise be forced into pure dead-reckoning.

Fig. 5 illustrates the variation in available satellites when including or excluding signals affected by ionospheric delay and bending at these altitudes. As the vehicle reaches higher layers, the number of satellites whose relative geometry forces the signal to travel through the ionosphere oscillates between zero and three. During these periods, the inclusion of these tracked satellites, despite their associated error, provides the necessary observations to prevent filter divergence.

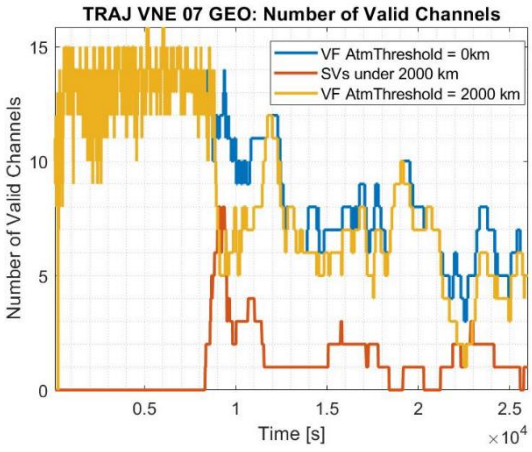

Fig. 5: Number of available GNSS satellites in GEO trajectory.

3.4.4 Dual antenna

The navigation system is designed to interface with multiple antenna inputs to ensure good performance the diverse mission and their different phases. In the current configuration, the NAVIGA-EVO unit simultaneously processes and hybridizes signals from two distinct antenna sources. During low-altitude operations, a geometric combined antenna is utilized, where the effective phase center is algorithmically derived from the relative positions of the dual-antenna setup.

As the vehicle ascends, the OBC manages the transition to a high-gain antenna optimized for high-altitude performance. This high directivity antenna reduces the main lobe coverage angle and is adapted for high altitude since the receiver is far away from Earth.

3.4.5 Dual frequency

When the GNSS receiver provides dual-frequency observables (e.g., L1 and L5), the architecture generates ionospheric-free measurement hybridization. This technique exploits the frequency-dependent dispersion of the ionosphere to eliminate first-order ionospheric effects delays, since the delay is inversely proportional to the square of the carrier frequency [3][22].

This combination is applied to both pseudorange and carrier-phase measurements, but it is not extended to Doppler observations, which remain frequency-specific. SIL results for the SR trajectory demonstrate that the application of ionospheric-free measurements effectively removes the ionospheric delay, resulting in a measurable improvement in both position and velocity estimation accuracy during the orbital and re-entry phases.

3.5 Enhanced Sensor Fusion: IMU+GNSS+STR

The unit integrates a multi-sensor fusion system, hybridizing attitude measurements from a STR. It is interesting to raise the question of which kind of hybridization architecture is going to be employed to fuse all the information provided by the multiple sensors present in this architecture: IMU, GNSS and STR.

The final architecture selected comprises multiple filters executed sequentially rather than in parallel. This approach was chosen due to its inherent flexibility and simplicity. The data fusion process must remain adaptable to user preferences, allowing for the selection of whether to hybridize the PVT solution (loose hybridization) or the raw measurements (tight hybridization) and, additionally, whether to include STR information in the fusion. Consequently, a separated filter architecture, as opposed to a unified design with a single sensitivity matrix of variable size, offers the most optimal and straightforward solution for accommodating diverse configurations.

The STR operates five times faster than the GNSS hybridization process. Therefore, if the data fusion hybridization combines GNSS tight measurements and STR measurements a frequency problem arises. GNSS latency can delay measurement acquisition by 200–300 ms, or even up to 500 ms. During this latency period, the STR may update the state two to five times. Therefore, by the time the tight GNSS measurement becomes available, the state may have already been updated multiple times.

In this work, it has been applied Larsen's correction to Alexander's method [14] which extends his approach [13]. Following Larsen's method, the star tracker and the tight hybridization work as two sequential filters. While the GNSS measurement is being processed, i.e. during the latency period, the STR continues hybridizing the inertial solution in parallel. [13] derives the optimal gain for fusing the delayed error measurement in the filter, ensuring that the covariance of the estimation errors remains optimal.

In the meanwhile, images of the stars that are taken in a moment of time, which are later processed and used for the computation of the attitude. This implies another small delay in time. However, this can

be corrected using extrapolation Larsen's approach [13] applied in a MEKF [12]. This is illustrated in Fig. 6.

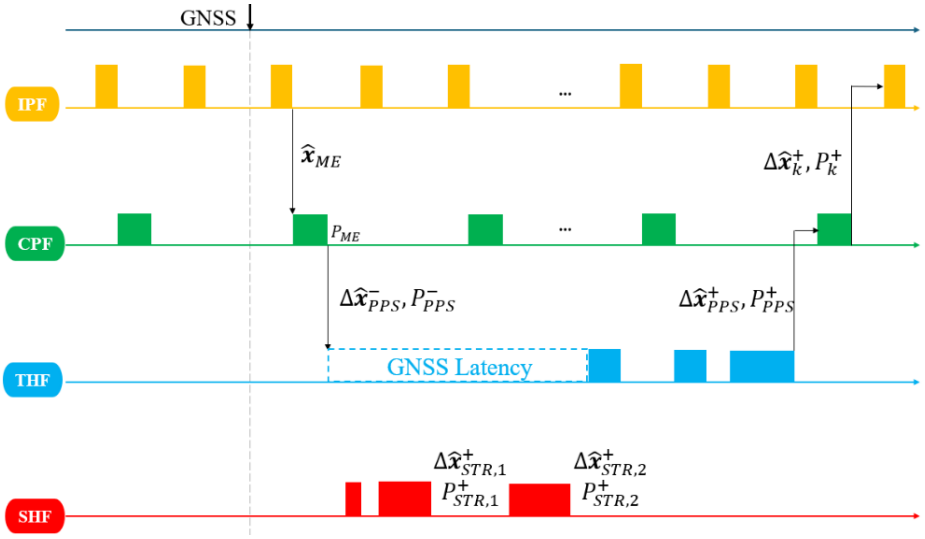

Fig. 6: Sequential architecture of DF functions with GNSS latency.

4 FDIR

The FDIR architecture is adapted to the specific hybridization scheme active within the data fusion framework. While the requirements for loosely coupled navigation are detailed in [2], the tightly coupled FDIR implementation is based on the logic established in [3][5], with specific adaptations for this mission profile.

However, the tightly coupled FDIR function is applied to the a-priori innovation, preventing individual or multiple faulty channels or divergent IMU propagation. The detection algorithms are applied independently to each measurement subset: PR, PRR and TDCP.

Complementing the GNSS checks, the STR FDIR architecture is structured as a multi-layered verification process. The primary layer leverages the internal diagnostic capabilities of the sensor, monitoring status flags and expected quality index of the measured quaternion to evaluate optical head status. The secondary layer applies innovation-based monitoring (similar to GNSS in [2]).

As the detailed characterization of these FDIR functions is outside the immediate scope of the performance results presented in this paper, an exhaustive description of the FDIR logic is omitted in favor of the primary navigation analysis.

5 Software Implementation

In the space sector, the capacity of the processors is very limited due to radiation tolerance and robustness. Given the specific constraints of the target microprocessor (single precision), early SIL testing identified numerical instabilities. This a challenge documented since the inception of Kalman Filtering and its application in the NASA Apollo program [18] and the limited capabilities of the Apollo guidance computer [24]. Even if, theoretically, the covariance matrix must remain symmetric and positive semi-

definite at all time, finite-precision arithmetic in embedded implementations can lead to a loss of positive definiteness.

This numerical sensitivity is further increased when the estimated uncertainties of certain state vector elements differ by several orders of magnitude. In this study, such conditions occur following the GNSS blackout phase during the Space Rider reentry and during segments of the Vega ascent to GEO when all raw GNSS signals are lost.

To mitigate these effects, a Square Root Extended Kalman Filter (SR-EKF) was implemented [18][24]. The SR-EKF improves numerical precision by propagating the Cholesky decomposition matrix (or equivalent square root) of the covariance matrix. This algorithm increases the precision of the filter and handles the covariance sensitivity matrix. Being P_k symmetric positive, then Σ_k is a matrix which exists and verifies:

$$P_k = \Sigma_k^T \Sigma_k \tag{6}$$

By propagating Σ_k, the condition number of the system is reduced to the square root of that of P_k, effectively doubling the effective precision of the computations. While the square root of a matrix is not unique [18], this architecture employs a QR-decomposition-based EKF [24]. Consequently, both the covariance propagation and the measurement update equations are reformulated to maintain the filter in square-root form throughout the navigation task. The SR-EKF implementation provides the numerical resilience necessary to handle the software issues associated to the limited microprocessor capacity.

6 Results

6.1 Simulation Setup and Methodology

In this section, the proposed navigation solution is presented, followed by a description of the employed setup and methodology. The proposed navigation solution was validated using a high-fidelity SIL environment implemented in MATLAB/Simulink. The simulation incorporates sophisticated sensor models and realistic trajectory profiles, accounting for mechanical shocks, vibrations, and the evolution of Earth Orientation Parameters (EOP) [25]. The data fusion algorithms are integrated via Simulink S-functions to ensure a representative execution of the flight software.

To assess the robustness of the highly configurable architecture, Monte Carlo campaigns were executed, each comprising 100 independent runs. These simulations vary critical IMU, GNSS, and STR error parameters. The following analysis evaluates performance across the two primary mission scenarios: the Vega trajectory to Geostationary Transfer Orbit (6.2) and the Space Rider reentry (6.3). The results presented in this paper provide a performance comparison for both mission scenarios under the different configurations discussed throughout this manuscript. The different Monte Carlo simulations are detailed in Table 2.

Table 2: Monte Carlo simulations mission cases.

Trajectory	Data Fusion Configuration	GNSS Model Configuration
GEO Injection	Loose (GHF)	Dual antenna, high-gain antenna >2000 km

GEO Injection	Tight (THF)	Dual antenna, high-gain antenna >2000 km
GEO Injection	Tight with STR (THF+SHF)	Dual antenna, high-gain antenna >2000 km
GEO Injection	Tight with STR (THF+SHF)	Dual antenna, omnidirectional antennas
Re-entry	Loose (GHF)	Single frequency
Re-entry	Tight (THF)	Single frequency
Re-entry	Tight with STR (THF+SHF)	Single frequency
Re-entry	Loose (GHF)	Dual frequency
Re-entry	Tight (THF)	Dual frequency
Re-entry	Tight with STR (THF+SHF)	Dual frequency

6.2 GEO Results

For the Vega mission, performance is assessed by comparing the estimated state (output of the SIL block) against the reference trajectory provided by ESA. Fig. 7 and Fig. 8**¡Error! No se encuentra el origen de la referencia.** depict the position and velocity error states, respectively, showing the 1st and 99th percentile envelopes (green and red curves) of the Monte Carlo simulations. The Monte Carlo error envelopes are plotted alongside their corresponding 3σ estimated state deviations to evaluate filter consistency, providing a direct comparison between the loose or NAVIGA configuration baseline (right plot) and tight (left plot) hybridization schemes.

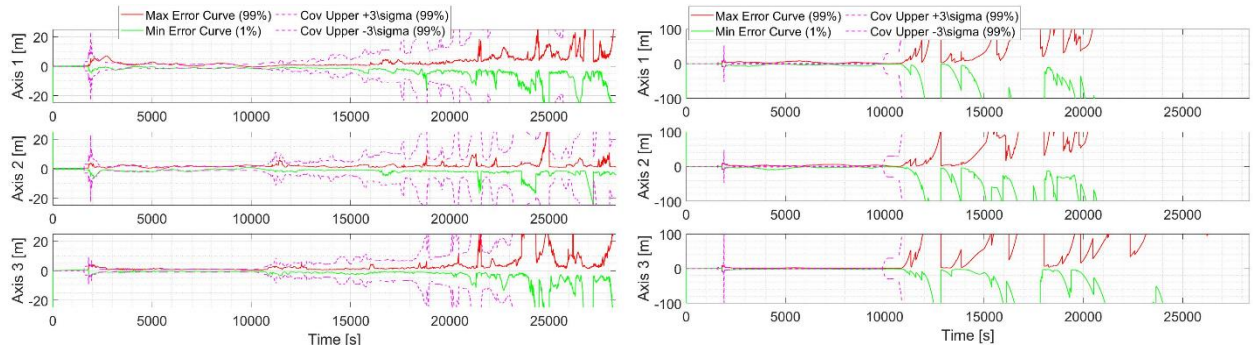

Fig. 7: Position error in Vega Trajectory to GEO with tight (left) and loose (right) hybridization.

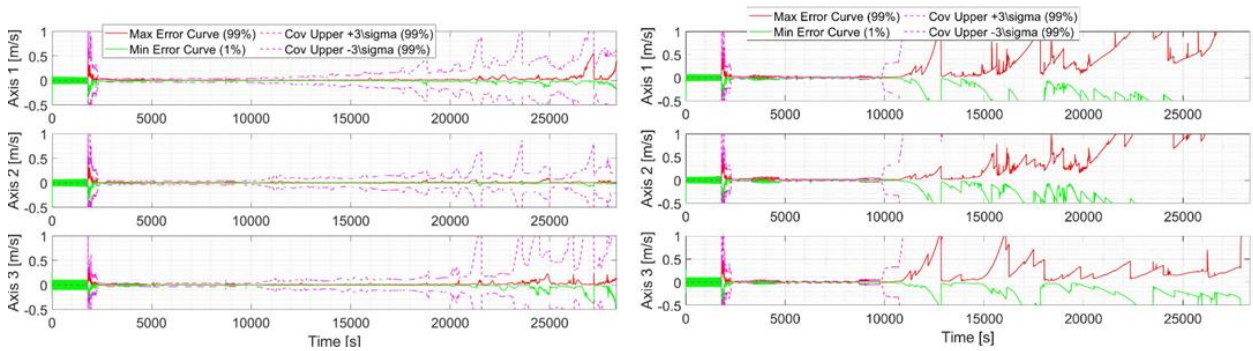

Fig. 8: Velocity error in Vega Trajectory to GEO with tight (left) and loose (right) hybridization.

A significant performance gain is observed with tight hybridization compared to the loose coupling approach. While the loose PVT solution requires at least four visible satellites to maintain a navigation fix, the tight architecture remains operational even with a single raw measurement. This advantage is particularly evident at high altitudes. As shown in Fig. 9 (right), while only two to three satellites are tracked, tight hybridization maintains accurate navigation where loose hybridization would revert to dead-reckoning. Even in Monte Carlo runs where GNSS signals are intermittently lost, the tight configuration constrains position errors to hundreds of meters, whereas loose coupling errors escalate into the kilometers. It is important to note that the Monte Carlo campaign includes specific iterations characterized by total GNSS signal outages. This is why, in these worst-case scenarios, even using tight hybridization the error is increased. Nevertheless, as illustrated in Fig. 9 (left plot), in scenarios where at least one space vehicle remains tracked throughout the entire trajectory, the tight hybridization architecture maintains high navigation accuracy upon arrival at GEO.

The dual-antenna strategy is further illustrated in Fig. 9. Below 2,000 km (10000 seconds of the simulations), the receiver combines signals at the RF level to ensure robustness during high angular rate maneuvers. Above this threshold, the system switches to a high-gain antenna. The tight hybridization framework facilitates the simultaneous and independent processing of raw measurements from both the high-gain and secondary antennas during this transition. This is because at these altitudes the relative azimuth of the satellites makes the antennas track different satellites. After this transition period, only the high-gain antenna operates. In case the GNSS constellation position allows the tracking of at least one satellite, it is possible to fuse the raw measurements. If the high-gain antenna is omitted (Fig. 10, right), the lack of satellite tracking leads to a rapid divergence in position error (position in Fig. 10, left) due to prolonged periods of dead-reckoning.

Monte Carlo analysis shows an important increase in performances when arriving at GEO. Nevertheless, the benefits of tight hybridization extend to low-altitude (NAVIGA) scenarios. The maximum error depicted in Fig. 7 and Fig. 8 is normalized and represented in Fig. 11. This figure illustrates that tight coupling reduces maximum position and velocity errors by over 50% compared to loose coupling. Furthermore, the integration of an STR significantly enhances attitude determination. While the STR has a marginal impact on position and velocity (Fig. 11), Fig. 12 demonstrates a substantial reduction in the norm of the maximum attitude error, as the STR provides direct observability that GNSS-only configurations lack.

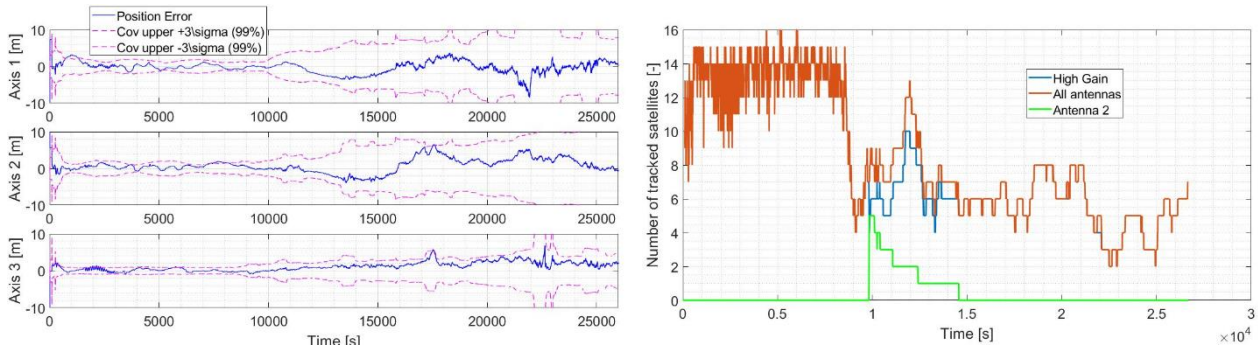

Fig. 9: Position error (left) and number of satellites (right) in Vega Trajectory to GEO using high-gain antenna.

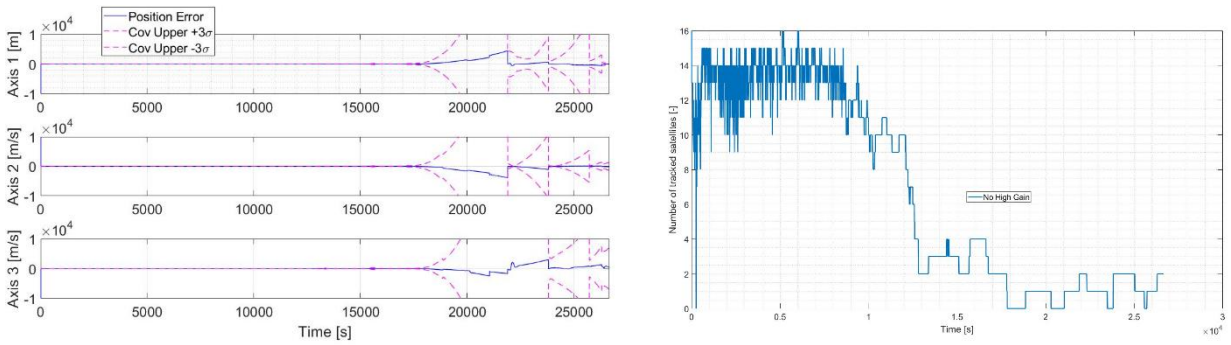

Fig. 10: Position error (left) and number of satellites (right) in Vega Trajectory to GEO without high-gain antenna.

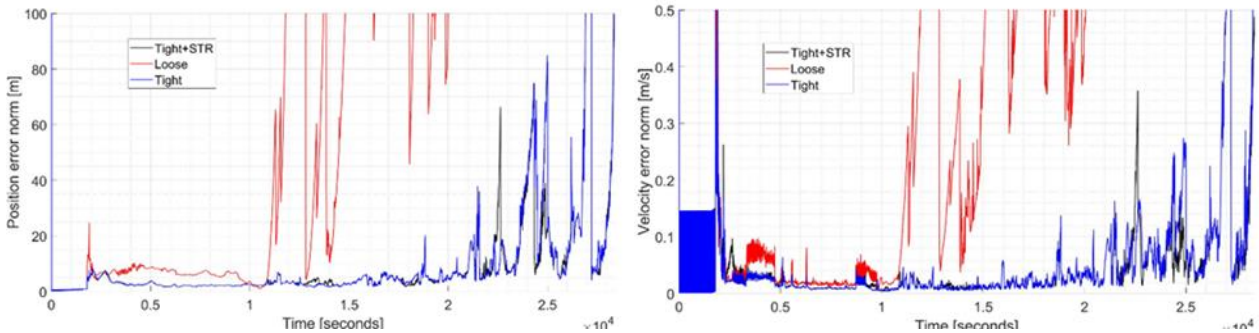

Fig. 11: Position and velocity maximum error in Vega Trajectory to GEO.

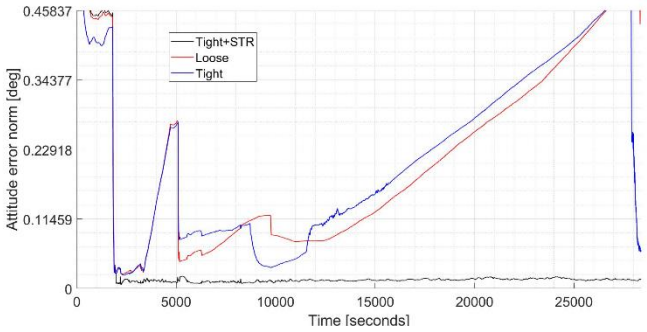

Fig. 12: Attitude maximum error in Vega Trajectory to GEO.

6.3 SR Results

The second analysis focuses on the SR reentry trajectory, comparing tight hybridization using single-frequency (L1) versus dual-frequency (L1/L5) measurements. The results are depicted in Fig. 13 (single frequency, L1) and Fig. 14 (dual frequency, L1/L5). Both figures show the 1st and 99th percentile of the Monte Carlo simulation of the position (right) and velocity (left) errors. The dual-frequency observables provide superior position estimation during both the orbital and reentry phases. Velocity estimation shows moderate improvement during the orbital phase but remains comparable during reentry.

Finally, it is performed a comparison of the three configurations plotting the norm of the Monte Carlo simulation worst case error (percentile 99th) in terms of position (Fig. 15, right) and velocity (Fig. 15,

left). This comparison takes place for the single-frequency measurement acquisition. Again, confirms that the tight architecture (equivalent for Tight+STR) yields the lowest error norms across all phases. During the high-dynamic reentry phase, the velocity estimation performance of all tight configurations converges, providing a stable and robust solution and slightly better than loose hybridization.

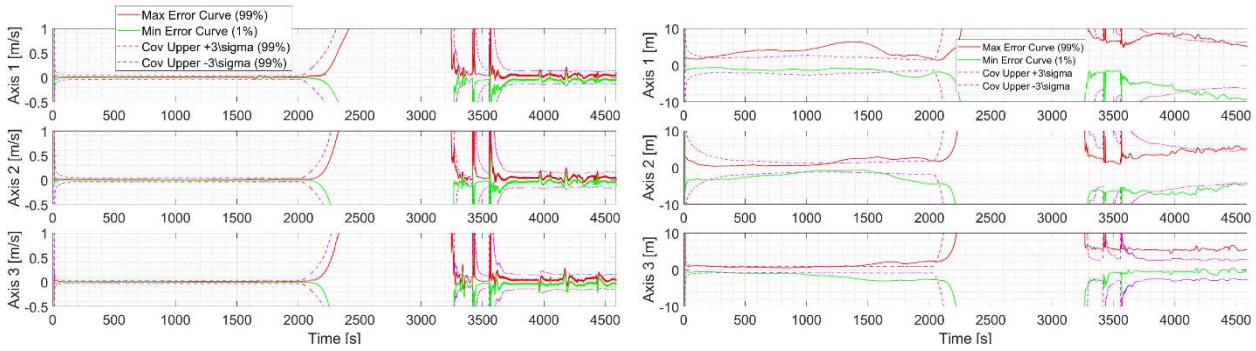

Fig. 13: Velocity (left) and position (right) maximum error in SR Trajectory (single frequency).

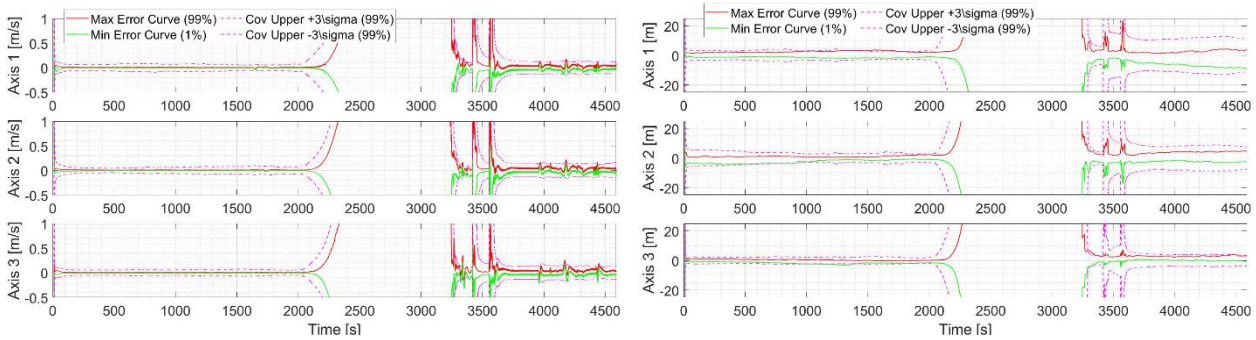

Fig. 14: Velocity (left) and position (right) maximum error in SR Trajectory (dual frequency).

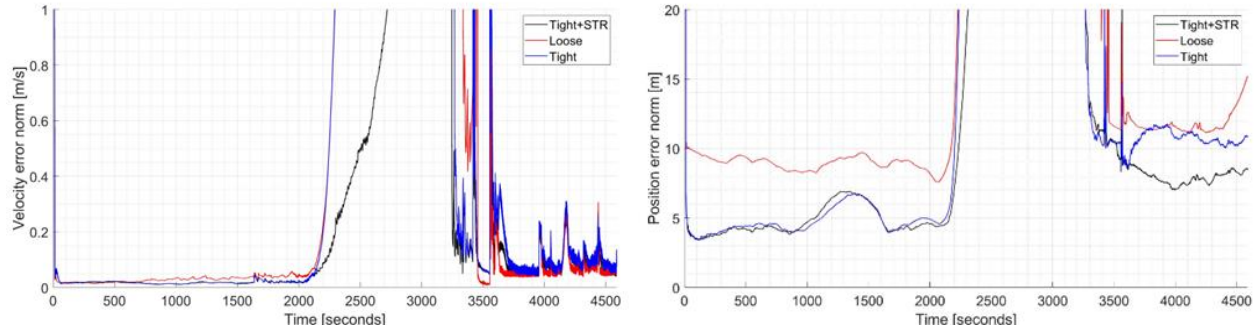

Fig. 15: Velocity (left) and position (right) maximum error in SR Trajectory (single frequency): Loose vs Tight vs Tight+STR.

6.4 Summary of Results

In this section, the performance of the NAVIGA-EVO architecture is summarized across the two reference missions to evaluate the performance of the new configuration with respect to the baseline loose configuration. Table 3 and Table 4 present maximum error of the 99th percentile from the Monte Carlo campaigns for the Vega and Space Rider trajectories, respectively, across the different mission phases. The most favorable performance results for each configuration are highlighted in bold to facilitate a direct comparison.

As detailed in Section 6.2, the Vega trajectory to GEO trajectory makes use of a dual-antenna configuration with the OBC logic to switch to a high-gain antenna for high-altitude segments. Table 3 indicates that the tightly coupled configuration significantly enhances performance compared to classical loose hybridization. During the missile and orbital phases, tight hybridization achieves a 50% reduction in maximum position and velocity errors (which was also observed in Fig. 7 and Fig. 8). Nevertheless, the most significant improvement occurs during the high-altitude phase. In this regime, as satellite geometry is often insufficient to maintain a standard PVT, the loose architecture diverges toward a dead-reckoning state with maximum errors exceeding 10000 m, whereas tight hybridization nearly achieves the same estimation performances as in low-altitude phase. The maximum error of 200 m is associated to Monte Carlo simulations in which no GNSS signals arrive to the receiver.

The analysis of the omnidirectional antenna configuration (without high-gain switching) shows identical performance to the high-gain setup at lower altitudes. However, at higher altitudes, while its position and velocity estimates are less accurate than the high-gain configuration, this setup still provides a measurable improvement over the loose solution by hybridizing the few available GNSS signals (Fig. 10, right).

Consequently, while the high-gain switching logic offers the best performance, the simpler omnidirectional configuration remains a viable alternative if mission requirements are less exigent. Furthermore, the integration of the STR is key for attitude estimation, constraining maximum errors to below 0.05 degrees and providing a significant enhancement in orientation accuracy relative to GNSS/IMU-only solutions. Being the combined Tight+STR (with high-gain antenna switching) the configuration with the best performances.

Table 3: Error in estimation in 99th percentile of Monte Carlo simulations in Vega Trajectory to GEO.

Navigation variable	Mission Phase	GEO Trajectory			
		Loose	Tight	**Tight+STR (high-gain)**	Tight+STR (omnidirectional)
Position [m]	Missile	25	8	**8**	8
	Orbital	10	4	**4**	4
	High Altitude	10000	200	**200**	5000
Velocity	Missile	1.0	0.5	**0.5**	0.5

[m/s]	Orbital	0.10	0.04	**0.04**	0.04
	High Altitude	10.0	0.3	**0.3**	3.5
Attitude [deg]	Missile	0.09	0.08	**0.05**	0.05
	Orbital	0.10	0.10	**0.05**	0.05
	High Altitude	1.15	1.15	**0.05**	0.05

In Section 6.3, the analysis of the Space Rider (SR) trajectory shows that the performance difference between loose and tight configurations is less pronounced. As shown in Table 4, tight coupling consistently improves position and velocity accuracy during the orbital phase, with the STR integration notoriously reducing the maximum attitude error.

The implementation of the dual-frequency configuration reduces maximum position errors in both the orbital and reentry phases. Interestingly, the transition to tight coupling during the reentry phase does not provide a significant performance gain over the loose architecture.

Therefore, the tight dual-frequency configuration provides the optimal performance for the Space Rider mission, even if the margin of improvement over single-frequency and even loose hybridization is narrowed during the reentry phase.

Table 4: Results for all configurations in SR Trajectory.

Navigation variable	Mission Phase	Single Frequency			Dual Frequency		
		Loose	Tight	Tight STR	Loose	Tight	**Tight STR**
Position [m]	Orbital	10	7	7	10	5	**5**
	Reentry	15	11	8	**9**	10	**10**
Velocity [m/s]	Orbital	0.06	0.03	0.03	0.06	0.03	**0.03**
	Reentry	0.3	0.3	0.3	0.3	0.3	**0.3**
Attitude [deg]	Orbital	0.6	0.6	0.06	0.6	0.6	**0.06**
	Reentry	0.4	0.4	0.4	0.4	0.4	**0.3**

7 Conclusions

This paper presents a comparative assessment between the newly developed NAVIGA-EVO navigation unit and the baseline NAVIGA configuration. The NAVIGA-EVO introduces an advanced and flexible hybridization architecture that integrates tight GNSS hybridization, GNSS dual-antenna processing, GNSS dual-frequency processing, and STR hybridization.

The obtained results clearly demonstrate the superior performance of the combined tight and STR architecture in terms of navigation accuracy and robustness. The dual-antenna processing enables precise navigation throughout the ascent to GEO orbit, while maintaining high accuracy levels, whereas the dual-frequency processing effectively mitigates position estimation errors during the SR re-entry phase.

Overall, the proposed tight hybridization architecture represents a significant advancement over the baseline loose hybridization scheme. It delivers enhanced versatility and compactness, substantially improving navigation performance in challenging GNSS environments, such as high-altitude and re-entry missions, and providing a robust a priori FDIR capability.

As described before, the current state of the project is the integration and simulation of the data fusion in software-in-the-loop. The roadmap of NAVIGA-EVO follows with the hardware in the loop simulations. From the original VNE project, a support equipment is used to perform DF and software verification, as well as hardware-in-the-loop testing. This support equipment has the capability of simulating tests with either simulated sensors or real stimulated sensors, allowing both phases of the VNE unit validation. Modifications such as the addition of STR sensor testing will be performed in order to enhance its testing and validation capabilities.

Finally, the NAVIGA-EVO will pass the environmental qualification, planned in 2027. Moreover, looking ahead, the EVO roadmap includes the integration of increasingly sophisticated technologies into the data fusion architecture, at least at simulation level. A primary objective is the incorporation of Differential GNSS hybridization, which will optimize the navigation during the reentry phase and enhance the final descent.

Declaration of Use of Artificial Intelligence

Artificial intelligence was not used in the work presented.

References

[1] Cacciatore, Francesco, Haya Ramos, Rodrigo, Tarabini Castellani, Lorenzo, Figueroa, Antonio, Veenman, Joost, Ramirez, S., Recupero, Cristina, Kerr, Murray, and Bejar, Juan. (2019). The Design of the GNC of the Re-entry Module of Space Rider.

[2] S. Ramirez, R. Polonio, S. de la Riva, C. Fernandez, S. Diaz, L. Favilli, G. Mattei, G. Curti. Robust FDIR approach for the future hybrid navigation system for VEGA-C. Proceedings of the 10th European Conference for Aeronautics and Space Sciences (EUCASS 2022), Lille, France, July 2022.

[3] Guilherme Fragoso Trigo. *Low-Cost Failure-Tolerant Hybrid Navigation Designs for Future Space Transportation Systems*. PhD thesis, University of Bremen, Bremen, Germany, Dezember 2020.

[4] Paul D. Groves. (2013). *Principles of GNSS, inertial, and multisensor integrated navigation systems* (2nd ed.). Artech House.

[5] G. F. Trigo, and S. Theil. Architectural Elements of Hybrid Navigation Systems for Future Space Transportation. *10th International ESA Conference on Guidance, Navigation & Control Systems*. Salzburg, Austria, May 2017.

[6] W. Jiang, D. Liu, B. Cai, C. Rizos, J. Wang, and W. Shangguan. A Fault-Tolerant Tightly Coupled GNSS/INS/OVS Integration Vehicle Navigation System Based on an FDP Algorithm. *IEEE Transactions on Vehicular Technology*, vol. 68, no. 7, pp. 6365-6378, July 2019. DOI: 10.1109/TVT.2019.2916852.

[7] Junchuan Zhou. *Low-cost MEMS-INS/GPS Integration using Nonlinear Filtering Approaches*. PhD thesis, University of Calgary, 2013.

[8] Junchuan Zhou, Stefan Knedlik, and Otmar Loffeld. (2012). INS/GPS for high-dynamic UAV-based applications. *International Journal of Navigation and Observation*, 2012. DOI: 10.1155/2012/678596.

[9] Jan Wendel, and Gert Trommer. Tightly coupled GPS/INS integration for missile application. *Aerospace Science and Technology*, 8(7), October 2004. DOI: 10.1016/j.ast.2004.07.003.

[10] Anthony Guillard, Paul Thevenon, and Carl Milner. Using TDCP Measurements in a Low-Cost PPP-IMU Hybridized Filter for Real-Time Applications. In *Proceedings of the 35th International Technical Meeting of the Satellite Division of The Institute of Navigation (ION GNSS+ 2022)*, Denver, Colorado, September 2022, pp. 2090-2103. DOI: 10.33012/2022.18331.

[11] E. J. Lefferts, F. L. Markley, and M. D. Shuster. Kalman filtering in spacecraft attitude determination. *AIAA 20th Aerospace Sciences Meeting*, AIAA-82-0070, Orlando, Florida, January 11–14, 1982.

[12] F. Landis Markley, and John L. Crassidis. *Fundamentals of Spacecraft Attitude Determination and Control*. Springer, 2014.

[13] T. D. Larsen, N. A. Andersen, O. Ravn, and N. K. Poulsen. Incorporation of time delayed measurements in a discrete-time Kalman filter. *Proceedings of the 37th IEEE Conference on Decision and Control (Cat. No.98CH36171)*, Tampa, FL, USA, 1998, pp. 3972-3977 vol.4. DOI: 10.1109/CDC.1998.761918.

[14] Harold L. Alexander. State estimation for distributed systems with sensing delay. In *Data Structures and Target Classification*, vol. 1470, 1991, pp. 103–111. DOI: 10.1117/12.44843.

[15] Ajit Gopalakrishnan, Niket S. Kaisare, and Shankar Narasimhan. Incorporating delayed and infrequent measurements in Extended Kalman Filter based nonlinear state estimation. *Journal of Process Control*, 21(1), 2011, pp. 119-129. ISSN 0959-1524. DOI: 10.1016/j.jprocont.2010.10.013.

[16] Stephen Steffes. Computationally Distributed Real-Time Dual Rate Kalman Filter. *Journal of Guidance, Control, and Dynamics*, 37 (3), 2014, pp. 1064-1068. DOI: 10.2514/1.G000179.

[17] Jay. A. Farrell. *Aided Navigation: GPS with High Rate Sensors*. McGraw-Hill, 2008.

[18] Dan Simon. *Optimal state estimation: Kalman, H infinity, and nonlinear approaches*. Wiley-Interscience, 2006.

[19] James Paul Collins. *Assessment and Development of a Tropospheric Delay Model for Aircraft Users of the Global Positioning System*. PhD thesis, University of New Brunswick, Canada, 1999.

[20] Oliver Montenbruck, and Eberhard Gill. Ionospheric Correction for GPS Tracking of LEO Satellites. *The Journal of Navigation*, 55(2), 2002, pp. 293-304. DOI: 10.1017/S0373463302001789.

[21] Norbert Zehentner. *Kinematic orbit positioning applying the raw observation approach to observe time variable gravity*. PhD thesis, Graz University of Technology, Austria, 2017. DOI: 10.13140/RG.2.2.33916.33927.

[22] Alfredo Renga, Ugo Tancredi, and Michele Grassi. Ionospheric Delay Handling for Relative Navigation by Carrier-Phase Differential GPS. *International Journal of Aerospace Engineering*, 2015, 570382, 8 pages, 2015. DOI: 10.1155/2015/570382.

[23] Mariano Wis, Enrique Santiago, Antonio Fernández, Pedro F. Silva, Ricardo Prata, Rui Nunes, and José Antonio García Molina. Results on use of GNSS for High Altitude Orbital Missions. *Proceedings of the 31st International Technical Meeting of the Satellite Division of The Institute of Navigation (ION GNSS+ 2018)*, Miami, Florida, September 2018, pp. 1710-1721. DOI: https://doi.org/10.33012/2018.15897.

[24] Kevin Tracy. A Square-Root Kalman Filter Using Only QR Decompositions, 2022. DOI: 10.48550/arXiv.2208.06452.

[25] Gérard Petit, and Brian Luzum. Transformation between the International Terrestrial Reference System and the Geocentric Celestial Reference System. *IERS Conventions (2010),* IERS Technical Note No. 36 Chapter 5, August 2012.